



Full paper

Sliding non-contact inductive nanogenerator

Wei-Zhi Song^{a,1}, Xiao-Xiong Wang^{a,1}, Hui-Jing Qiu^a, Qi Liu^a, Jun Zhang^a, Zhiyong Fan^b, Miao Yu^{a,c}, Seeram Ramakrishna^{a,d}, Han Hu^e, Yun-Ze Long^{a,*}^a Collaborative Innovation Center for Nanomaterials & Devices, College of Physics, Qingdao University, Qingdao, 266071, China^b Department of Electronic & Computer Engineering, The Hong Kong University of Science & Technology, Kowloon, Hong Kong, China^c Department of Mechanical Engineering, Columbia University, New York, NY, 10027, USA^d Center for Nanofibers & Nanotechnology, National University of Singapore, Singapore^e State Key Laboratory of Heavy Oil Processing, College of Chemical Engineering, China University of Petroleum (East China), Qingdao, 266580, China

ARTICLE INFO

Keywords:

Energy harvesting
Non-contact
Inductive nanogenerator
High conversion efficiency

ABSTRACT

Nanogenerators generate power by inducing charge moving between the electrodes after charge generation. Using this principle, all the generated charges have the potential to design nanogenerators. In this work, we designed a new configuration that can generate power by electrostatic induction in a universally applicable way. The conversion efficiency of the contact and non-contact configuration was compared and it was found that the output capability of the non-contact inductive nanogenerator (NCING) did not decrease significantly. In addition to the traditional triboelectric non-contact mode and electret induced power generation, it was found that this configuration is applicable to more charge-induced power generation, so we directly used a charged capacitor to complete the induction power generation, which has not been reported yet. Through these experiments, we have proven the powerful ability of the free sliding non-contact configuration. In future research, the charge source can be replaced with other ones. By controlling the fixed charge to generate a higher potential, the output can be improved. Therefore, this wide-applicable generation mechanism has a huge impetus to the design of new nanogenerators.

1. Introduction

In the nano field, nanogenerators have received much attention. In the course of more than ten years of development, triboelectric nanogenerators [1–7], piezoelectric nanogenerators [8–16], pyroelectric nanogenerators [17–20] and electrostatic nanogenerators [21] have emerged. These nanogenerators do not require the use of heavy metals and are more environmentally friendly. Biocompatible materials can be used so that the generators can power up the devices on human skin or inside the human body [22]. These nanogenerators can be used in a variety of self-powered systems such as sensors [23–25], robotics [26–28], electromechanics [29,30], electronics [31] and tumor therapy [32]. These nanogenerators will replace the use of batteries in nano systems, contributing to smaller size and better safety of the system.

In general, nanogenerators can be divided into two categories, namely contact nanogenerators and non-contact nanogenerators. For contact nanogenerators, charges are collected by a certain means like friction, pressure or heat. Then the aggregated charges induce the variation of electric potential on the electrode through electrostatic

induction to complete the power generation process [33,34]. For non-contact nanogenerators, net charge or polarization is formed first by some means, and the carrier of charge or polarization were then formed a relative motivation between electrodes, while the load or meter can be linked between the electrodes. In this configuration, the conversion efficiency can be greatly improved, but the peak output dropped simultaneously [35–38].

Here we systematically compare the performance of contact nanogenerators and non-contact nanogenerators, as well as the conversion efficiency comparison between the contact and non-contact modes of the traditional electret charges and friction induced charges. Also we found that the non-contact configuration will lead to the design of a series of new nanogenerators, where a charged capacitor was demonstrated capable as a charge source to generate power. The NCING can illuminate LEDs or power small electronic devices and successfully collect water wave energy. An inertial sensor basing on the NCING can also be designed.

* Corresponding author.

E-mail address: yunze.long@qdu.edu.cn (Y.-Z. Long).¹ Co-first author.

2. Experimental section

2.1. Materials

PVDF powder (Mw ~550000, Shanghai 3F New Material Co., Ltd.) was used in this work. N, N-Dimethylformamide (DMF) was obtained from Sinopharm Chemical Reagents. Acetone was obtained from the Laiyang Fine Chemical Factory, China. Nylon 6 (PA6) powders was supplied by Macklin Biochemical Co., Ltd., China. Formic acid and acetic acid were obtained from Sinopharm Chemical Reagent Co., Ltd.

2.2. Preparation of solutions for electrospinning

A PVDF solution was prepared by dissolving PVDF powder (22 wt %) in an acetone–DMF solvent mixture (1/1 w/w) and then stirring the mixture with a magnetic stir bar for 4 h at 50 °C. For preparation of the PA 6 transparent solution with a concentration of 15 wt %, dissolving the polymer in formic acid-acetic acid (1/1 w/w) and was continuously stirred for 4 h at room temperature.

2.3. Fabrication of the NCING

The NCING employs a non-contact sliding tape nanogenerator design with various charge sources. It consists of two parts, a charge source and two electrodes, as show in Fig. 2a. The charge source can be PVDF electret, parallel plate capacitor or friction-charged nylon (Fig. 2b). The PVDF electret and nylon were produced by electrospinning. The capacitor was a gold-plated glass plate on both sides. The charge source and the electrode were respectively fixed between two objects which can generate relative displacement and do not contact each other, thereby forming an NCING.

2.4. Characterizations

The morphology and the microstructure of the PVDF and nylon were characterized by scanning electron microscopy (SEM, TM-1000, Hitachi). The crystalline structures of the PVDF electret were determined by Raman spectrum (Labram HR 800, Jobin-Yvon Horiba, France). The output short current of NCING was tested by a

picoammeter (Keithley 6487). The open-circuit voltage of NCING and the charging voltage of capacitor was recorded by a digital multimeter (Rigol DM 3058). An infrared camera (FLIR AX8) was used to characterize the change in temperature of the functional material of the nanogenerator after induction and friction. A homemade device was used to create a non-contact reciprocating motion.

3. Results and discussion

3.1. Device and characterization

Fig. 1 shows the basic configuration of a testing system. The electromagnetic drive drives the reciprocating mechanism such that the charge source ($1 \times 8 \text{ cm}^2$) which was fixed on an insulated reciprocating rigid platform moves in the vicinity of the two adjacent electrode plates, and the electrode plate acts as a power supply electrode to drive an external load or test instrument. Taking the electret as an example, as shown in Fig. 1b, a typical electret retains fixed polarization strength such that the region near one pole exhibits negative potential and the region near the other pole affords positive potential. This potential increases as the polarization increases and decreases significantly with increase of distance. A single sensing electrode forms an equipotential body in this electric field. However the positions of the two electrodes are different with respect to the electret. More specifically, the potential of the adjacent electrode is larger, and the electrode at the far side is closer to zero potential. As a result, typical potential difference is formed between the electrodes, and a continuous current is generated to power the device when an external load is connected. Fig. 1c shows an SEM photograph of the electret used: electrospun PVDF nanofiber membrane.

3.2. Working mechanism and calculation analysis

The type of the NCING is based on the inductive power effect between a charge source and electrodes (Fig. 2a). So the type of charge source is not fixed, all charged bodies will be possible, like capacitors and friction-charged nylon (Fig. 2b). When the negatively charged source is close to the aluminum electrode, the induced electrification effect causes a positive charge on the electrode. When the charge source

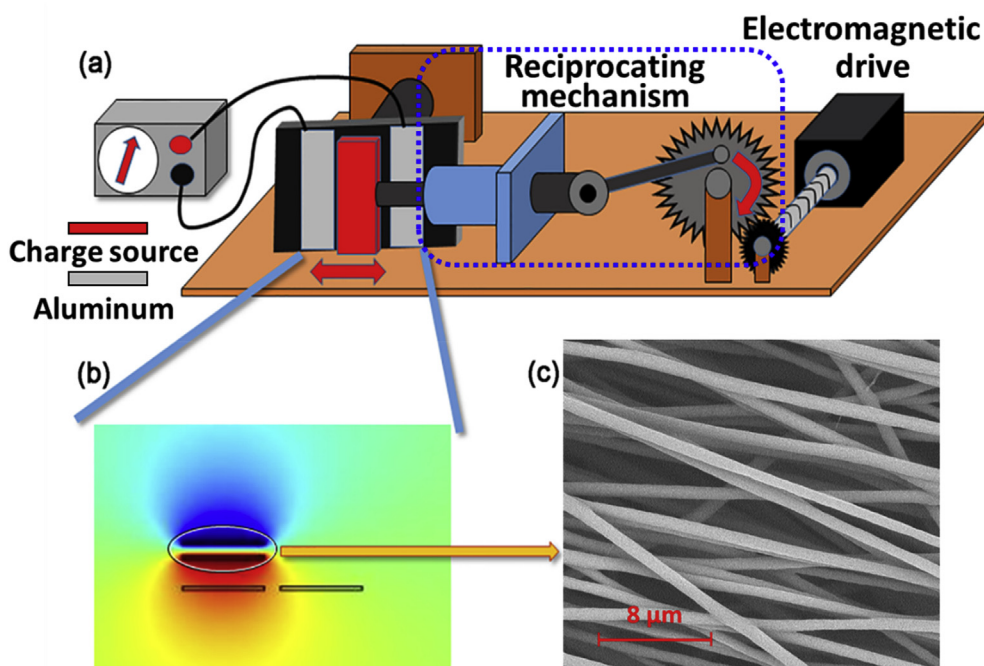


Fig. 1. (a) Schematic diagram of the test device for inductive electrification, (b) schematic diagram of the electric field distribution of the inductive electrification function region, red indicates positive potential and blue indicates negative potential. (c) SEM image of the used electret (electrospun PVDF nanofibres). (For interpretation of the references to colour in this figure legend, the reader is referred to the Web version of this article.)

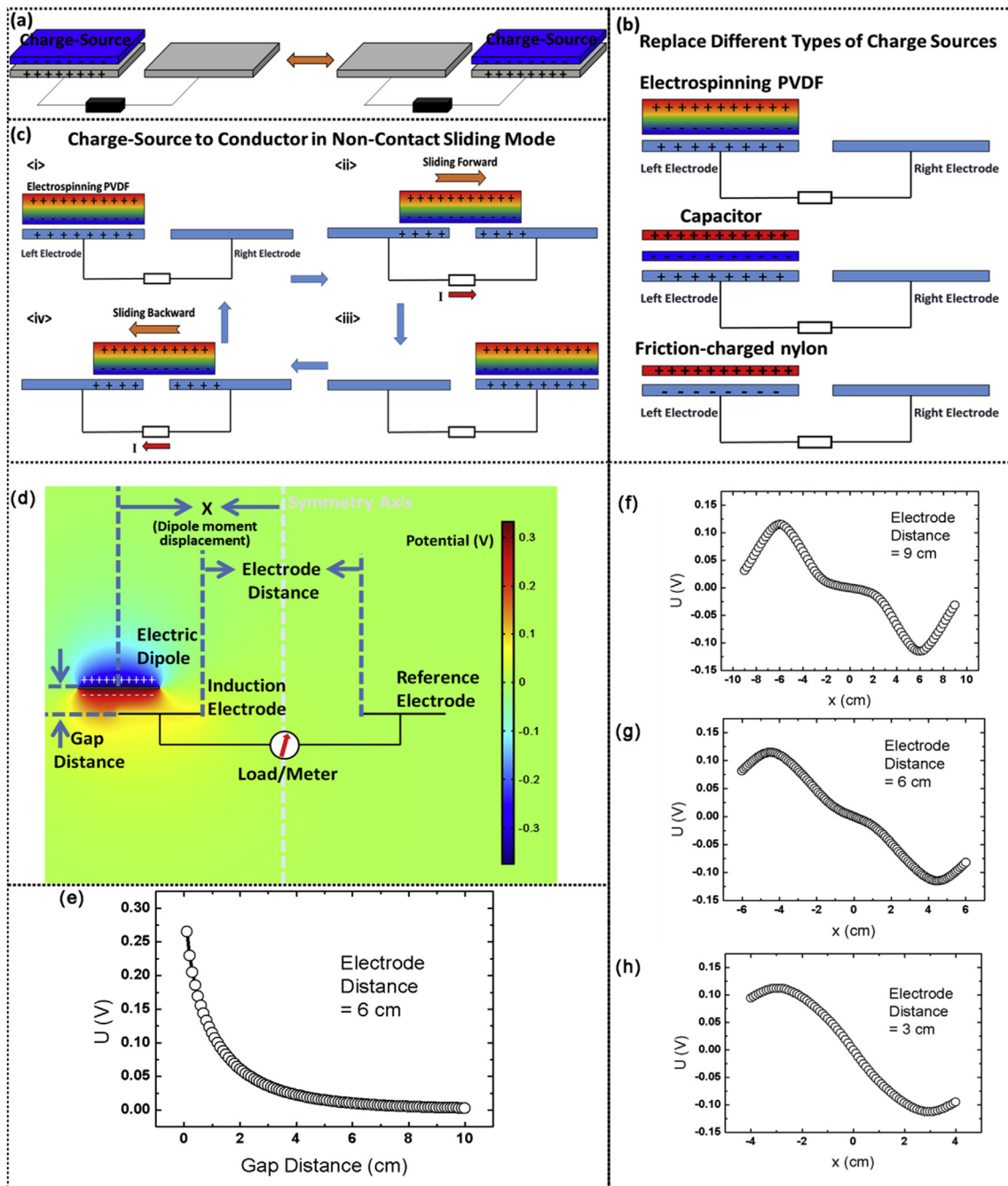


Fig. 2. Working mechanism and finite element calculation and analysis of the induced electrification. (a) Basic elements of an NCING. (b) Demonstration of replacing the charge source by capacitor or free charge. (c) Working mechanism of electret inductive nanogenerator in the non-contact sliding mode. (d–h) Simulation results using electret as an example. (d) A typical simulation result of the electric potential distribution in space and parameter names. (e) Changing of the voltage difference between the two electrodes as a variation of the gap distance between the electric dipole material and the induction electrode. (f–h) Changing of the voltage difference between the two electrodes as a variation of the electric dipole material position, and the electrode distance are 9 cm, 6 cm and 3 cm correspondingly.

is just above the first electrode (e.g., the left electrode as shown in Fig. 2c < i >), all the positive charges in the ring are attracted to the upper surface of the left electrode (LE). Then, when the charge source slides toward the right electrode (RE) (Fig. 2c < ii >), in order to shield the non-local field-negative charge on the dielectric, the positive charge in the loop will flow from the LE to the RE through the load. When the charge source is just above the RE (Fig. 2c < iii >), all positive charges are driven to RE. After that, when the charge source slides in the reverse direction from RE to LE, a positive charge flow is driven in the same direction and a reverse current is generated in the load (Fig. 2c < iv >) [38]. This is a complete electricity generation cycle.

We also simulated the electret-induced electrification using COMSOL software. Typical results are shown in Fig. 2d. Both the electret and the electrodes were set to a thin plate of 3 cm * 3 cm * 0.05 cm. The electric displacement field was set to 25 nC m⁻². We first fixed the electrode distance at 6 cm, and studied the variation of the induced electrification voltage with the distance between the charge source and the electrode, as shown in Fig. 2e. It can be seen that as the gap distance decreases, the induced voltage rapidly increases. At long distances, the voltage generally shows a reciprocal growth trend with decreasing distance, although this growth rate tends to slow down as the electrode approaches. According to the basic principle of

electromagnetics, at a closer position, the surface charge satisfies the in-plane translational symmetry, and the potential will show a linear change with distance. When the distance between the two electrodes are far enough, the electret has less influence on the reference electrode. As a result, the electret only affects the nearby electrode, resulting in an independent positive and negative wave pattern as shown in Fig. 2f. As the electrode spacing decreases, two independent potential response signals will overlap each other, as shown in Fig. 2g and h. Since the induced potential at the electrode attenuates with distance intensely, this signal superposition does not cause a significant maximum potential change, but only a change in the voltage wave mode as scanning electric dipole position x . Since the polarization is a combination of positive and negative charges, it can be inferred that if the charge source is changed to an independent positive or negative charge, the corresponding response potential will be more pronounced. So we also performed simulations using such charges and relative results are put in the supporting information, as shown in Fig. S6.

3.3. The electrical performance of NCING

First, we replaced the charge source to an electrospun nylon film and charges were generated by friction with PVDF. Fig. 3a is the schematic diagram of electric field distribution of nylon film before and after friction with PVDF. It can be seen that the surface potential of nylon is significantly improved after friction with PVDF. Fig. 3b is the short current of the NCING with electrospun nylon film as a charge source. Since nylon is prepared by electrospinning, residual charge is thus on the film which contributes to a small output before friction with

PVDF. After friction with PVDF, the amount of charge on the nylon film increased, resulting in more charge on the electrode. It is easily to find that the output is increased by 4 times from Fig. 3b. Fig. 3c is the charging curve by the NCING with frictionally charged nylon as charge source. The voltage can reach 1.8 V, sufficient to power some small electronic devices or LED, as shown in Fig. S3, Video S1 and Video S2 in the supporting information.

Supplementary video related to this article can be found at <https://doi.org/10.1016/j.nanoen.2019.103878>.

And then, based on the NCING, a single pendulum model (Fig. S8a) was designed to facilitate the calculation of energy conversion efficiency and control the input work. The nylon rubbed with PVDF is fixed at the lower part of the block as a charge source, and the electrode is fixed on the bottom plate. Each time the block is pulled to the same height and then released, the charge source can swing back and forth on the electrode. We also systematically studied the dependence of output current on load resistance in this mode. It was found that the current (the values quoted are peak instantaneous values) exhibited a reversely proportional relationship with the elevation of load resistances, as diagrammed in Fig. 3d. Under the condition that the pendulum mass is 10 g and the wobble frequency is 0.8 Hz, the maximum load peak power is $21 \mu\text{W}/\text{m}^2$ with the relative load peak current is 7.8 nA, when the external load resistance is 350 Ω .

Although the output power is lower than the TENG of some papers [39], in practical applications, the output of the nanogenerator needs to be adjusted and stored for use when the load electronics require energy. Therefore, as can be seen from Fig. 3c, NCING is similar to TENG [39] in the ability to charge capacitors. Moreover, we also noticed that from

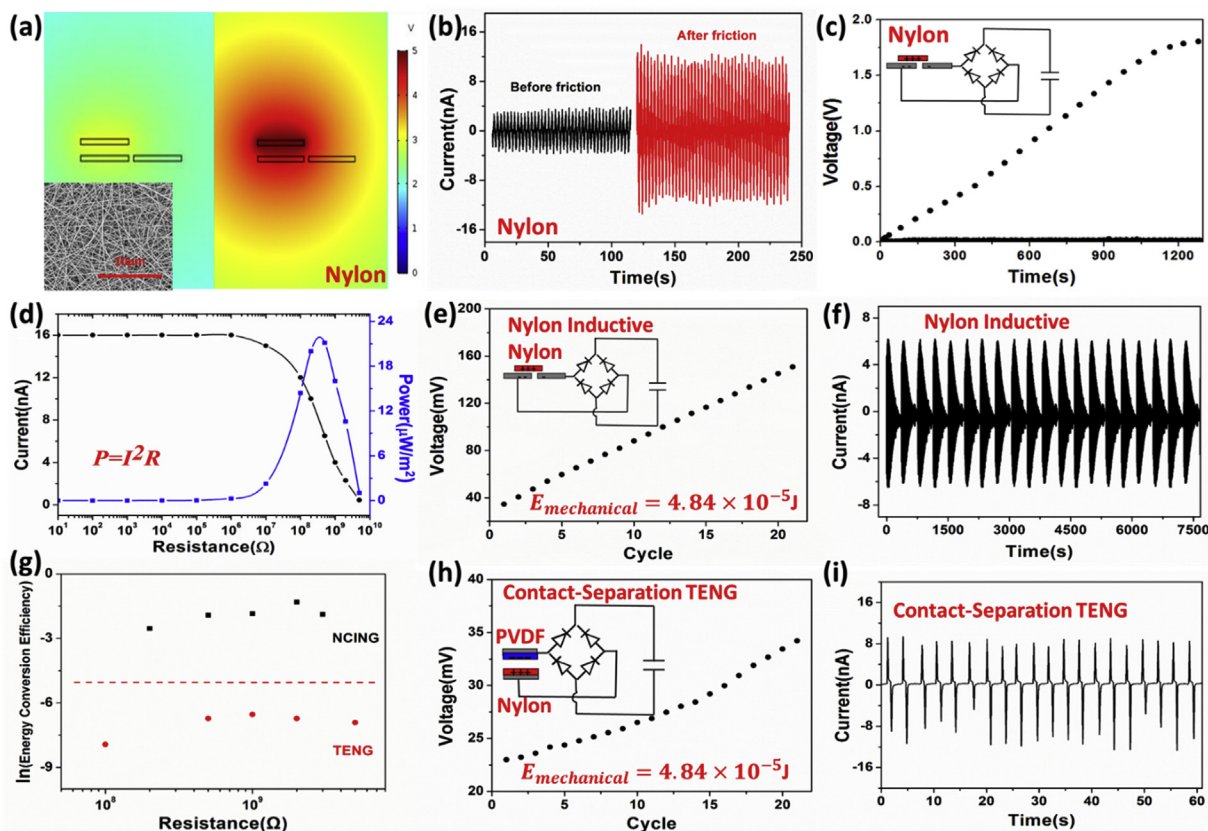


Fig. 3. (a) Schematic diagram of electric field distribution of nylon film (before and after friction with PVDF). Red indicates positive potential and blue indicates negative potential. (b) The short current of the NCING with electrospun nylon film (before and after friction) as a charge source. (c) Charging curve by the NCING with frictionally charged nylon as charge source. (d) Measured output current and output power with variable load resistances. (e) Charging curve of a 47 μF commercial capacitor by the NCING of simple pendulum mode in 20 cycles, and (f) the short current during charging. (g) The comparison of energy conversion efficiency between NCING and TENG with variable load resistances. (h) Charging curve of a 47 μF commercial capacitor by the contact-separation TENG in 20 cycles, and (i) the short current during charging. (For interpretation of the references to colour in this figure legend, the reader is referred to the Web version of this article.)

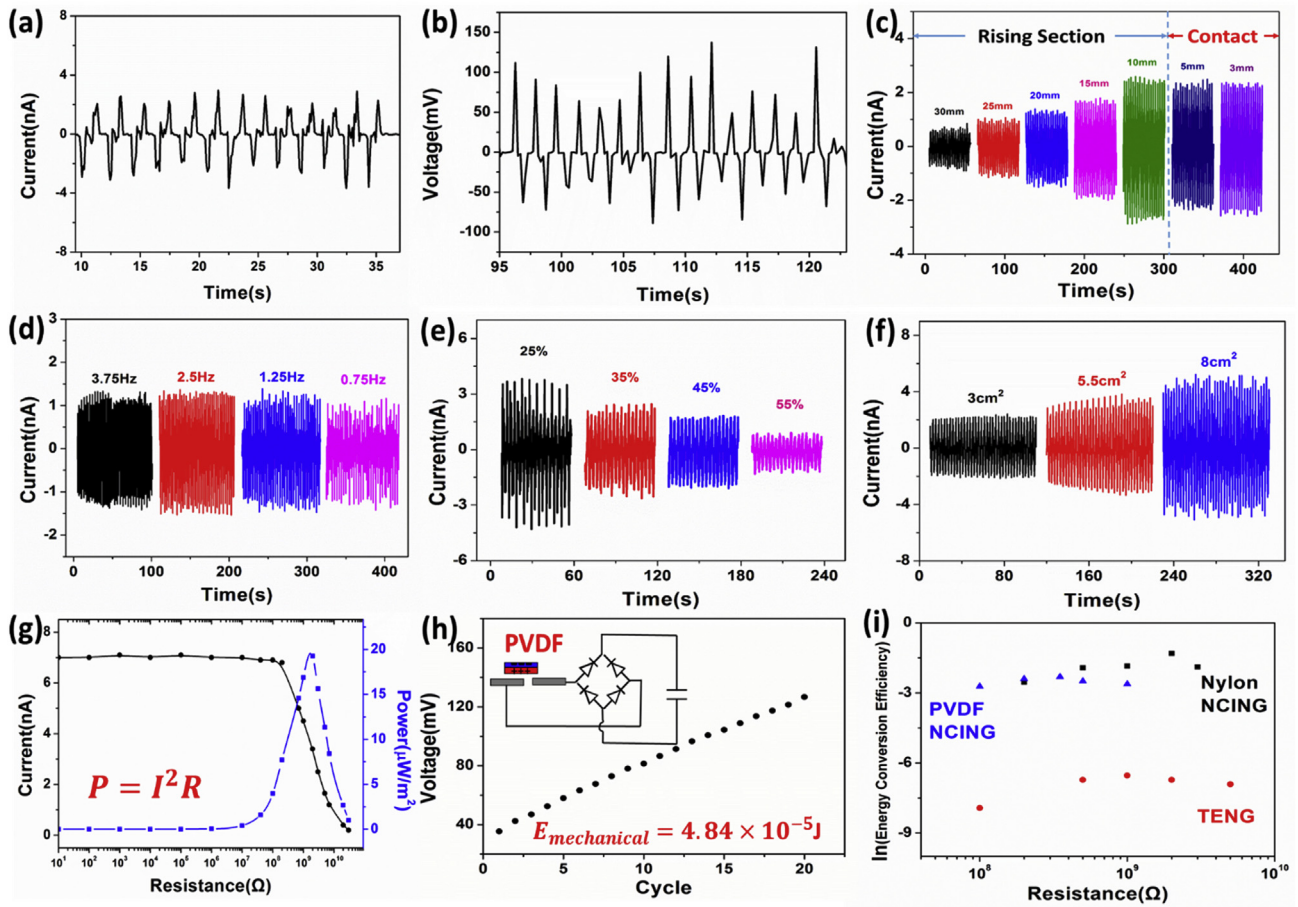


Fig. 4. The output of PVDF electret NCING under different conditions. (a) Typical output short current, (b) output open-circuit voltage of the PVDF electret NCING. Output short current under (c) different distance between the electret and the electrode, (d) different moving frequency, (e) different ambient humidity, and (f) different membrane areas. (g) Measured output current and output power with variable load resistances. (h) Charging curve of a 47 μF commercial capacitor by the NCING of simple pendulum mode in 20 cycles. (i) The comparison of energy conversion efficiency between NCING and TENG with variable load resistances.

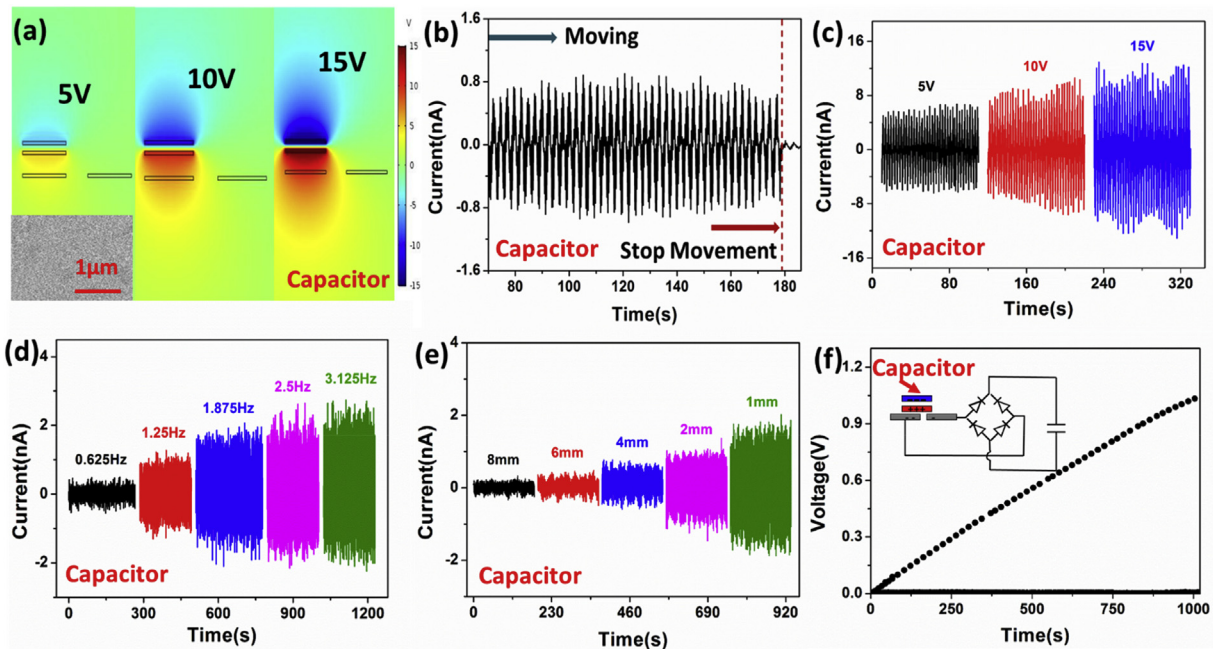


Fig. 5. (a) Schematic diagram of electric field distribution of parallel plate capacitor with different voltages. (b) The output current when using a capacitor as a charge source, (c) the capacitors with different voltages, (d) different moving frequency, (e) different distance between the capacitor and the electrode. (f) Charging curve of a 47 μF commercial capacitor by the NCING with capacitor as charge source.

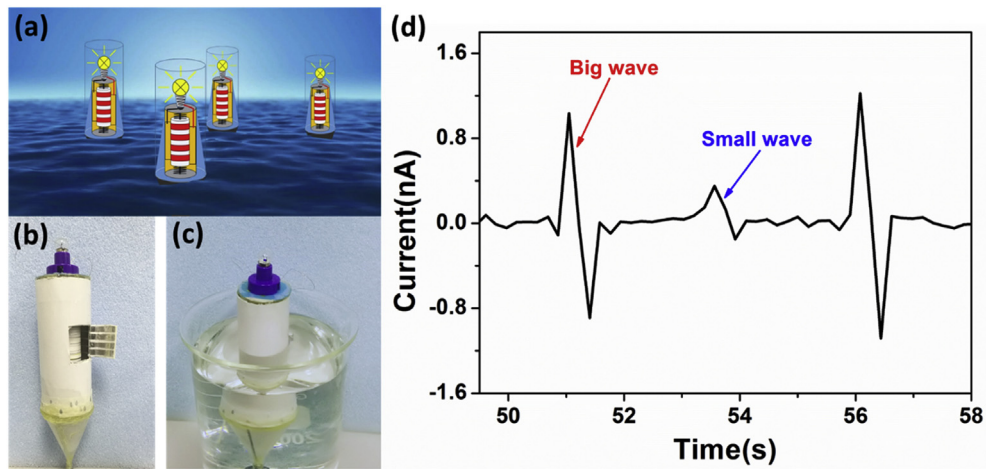


Fig. 6. (a) Water wave energy collection system based on NCING and used for illumination and indication. (b–c) Digital pictures of the home-made water wave energy collection device. (d) Current output waveform when the system collects water waves.

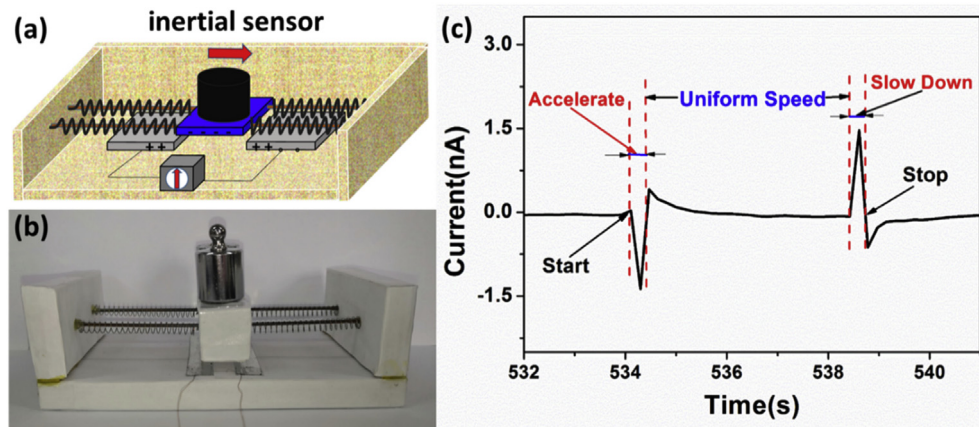


Fig. 7. (a) A schematic diagram of inertial sensor based on NCING. (b) The photograph of inertial sensor and (c) its output waveform.

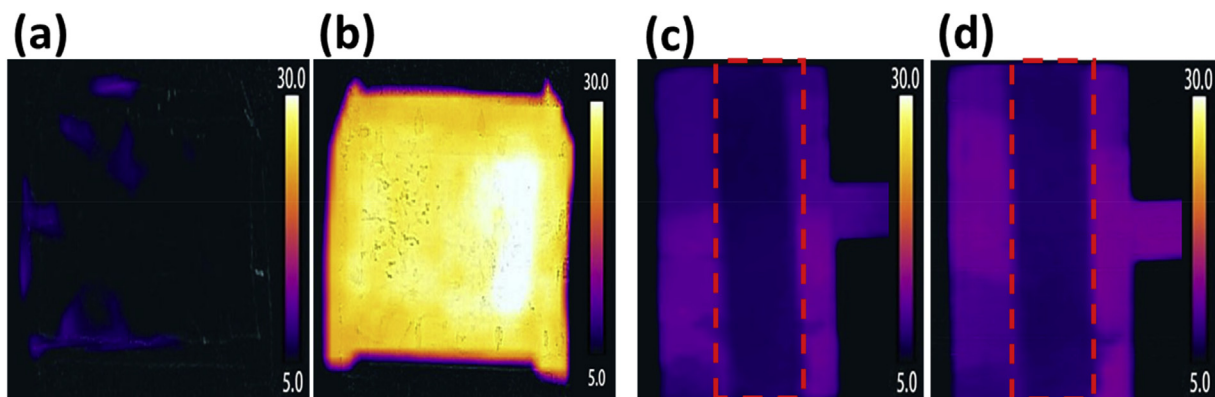


Fig. 8. (a–b) Infrared thermography image of PVDF film before and after friction with aluminum foil for 2 min (c–d) Infrared thermography image of PVDF electrets before and after NCING work for 2 min.

the comparison of Fig. 4a and Fig. 3i, the single peak width of NCING is significantly wider than the single peak of TENG, and the amount of charge after integration is of the same order of magnitude, as shown in Fig. S9. On the other hand, it is clear that as frequency and force increase, the output power of TENG rises because the input power of the system increases. Therefore, it is more advantageous to use a Root Mean Square (RMS) value instead of just using the instantaneous peak power output for a given period of time to see the ratio between the input and output power through the system [40].

In order to better describe the performance of NCING, we compared the ability of NCING with single-swing mode and contact-separated TENG to charge capacitors under the same input power. The pendulum has a pendulum length of 40 cm and the starting point of each cycle is 2° off center until the swing stops. The weight of the pendulum is 10 g, and the cycle is 20 times (the cycle of the single pendulum model is from the start of the swing until the motion stops), so the input power of the system can be calculated as:

$$E_{\text{mechanical}} = N \cdot mgh \quad (1)$$

$$h = L - L \cos \theta \quad (2)$$

where N is the number of cycles, so N is equal to 20, m is the weight of the pendulum, $g = 9.8 \text{ N/kg}$, L is the length of the pendulum, θ is the angle of the pendulum swing (as shown in Fig. S8b). So the E_m is about $4.84 \times 10^{-5} \text{ J}$. We put the same work on TENG. The comparison results are shown in Fig. 3e and h. After 20 cycles, NCING charges the capacitor for 116 mV (from 34 mV to 150 mV). TENG charges the capacitor for 11 mV (from 23 mV to 34 mV). Therefore, under the same conditions, the energy conversion efficiency of NCING is greater than that of TENG. Fig. 3f and i shows the current curves of NCING and TENG during 20 cycles, respectively. The highest power output of one cycle during the measurement is shown in Fig. S10. The overall generated electrical power under one cycle can be calculated as:

$$E_{\text{electrical}} = \int I^2 \cdot R \cdot dt \quad (3)$$

where I is the instantaneous current, R is the load resistance. Then the energy conversion efficiency of the NCING under different loads was calculated as:

$$\eta = \frac{E_{\text{electrical}}}{E'_{\text{mechanical}}} = \frac{\int I^2 \cdot R \cdot dt}{mgh} \times 100\% \quad (4)$$

where $E'_{\text{mechanical}}$ is the mechanical energy of one cycle. The result as shown in Fig. S11a, the energy conversion efficiency is about 27% at a load of $2 \text{ G}\Omega$ (air resistance causes huge loss of energy). The energy conversion efficiency of Contact-Separated TENG also was tested in the same way, as shown in Fig. S11b. In order to compare the energy conversion efficiency of NCING and TENG more intuitively and conveniently, their energy conversion efficiencies was taken logarithm, as shown in Fig. 3g. It is easy to see that the energy conversion efficiency of NCING is greater than that of TENG.

The representative electrical output capability of PVDF electret NCING is presented in Fig. 4a–f. Fig. 4a and b are the typical short current and open-circuit voltage. Fig. 4c shows the output current at different distance between the PVDF electret and the electrode. It can be found that the output gradually increases as the distance decreases. When the distance is less than 5 mm, the output does not continue to increase, but tend to saturation. In the case where the sliding frequency is changed at the same distance, the output also increases with the frequency increases, but is less noticeable, as shown in Fig. 4d. The most serious factor affecting output performance is humidity. The output increases sharply with humidity decreasing, as shown in Fig. 4e. The reason is that, as the humidity increases the water molecules in the air will affect the surface charge density of the charge source [41], resulting in a decrease in the charge induced on the electrode and a decrease in output. Fig. 4f shows the output in the case of three different membrane areas (3 , 5.5 and 8 cm^2) of charge source. With the area of the charge source film increases, the amount of charge induced on the electrode also increases. When the sliding frequency is constant, the amount of charge passing through the unit area under unit time increases, giving rise to a larger current. We also tested the loop stability of NCING and the effect of temperature on the output, as shown in Figs. S12 and S13. NCING has shown good stability.

Similarly, PVDF electret-based NCING has also been tested for output current and output power and energy conversion efficiency at different load resistances, as well as the ability to charge commercial capacitors, as shown in Fig. 4g–i. It can be seen from Fig. 4g that the dependence of the output current of NCING on the load resistance does not change significantly when the charge source is changed from nylon to PVDF electret. The peak instantaneous value of the current is inversely proportional to the increase of the load resistance. Although the current is reduced at low load resistance, the maximum load peak power is still kept at around $20 \mu\text{W}/\text{m}^2$. The reason is that the peak load resistance moves to the right. As for the charging capacity of

commercial capacitors, the same single pendulum model was used, and the same mechanical energy was input ($4.84 \times 10^{-5} \text{ J}$). After 20 cycles, the capacitor was charged with 99 mV (from 27 mV to 126 mV), as shown in Fig. 4h. Therefore, after changing the charge source, the NCING can still maintain a good charging ability.

Finally, the energy conversion efficiency of NCING based on PVDF electrets was compared with the NCING with a nylon charge source and contact separation TENG based on nylon and PVDF, as shown in Fig. 4i. It is easy to see that changing the charge source has little effect on the energy conversion efficiency of NCING. No matter which charge source NCING is selected, the energy conversion efficiency is higher than TENG. This fully proves that our NCING is universal.

Last but not least, the charge source was changed from PVDF electret to other charged objects like a plane-parallel capacitor (the capacitor was pre-charged to the specified voltage value) for induction of power generation. The result is shown in Fig. 5a–f. We used COMSOL to simulate the electric field distribution of the induced electrification function area when the capacitor with different charging voltages (5, 10 and 15 V) was used as the charge source, as shown in Fig. 5a. It is easy to find that the potential at the electrode position increases, which show the similar trend with the charging voltage of the capacitor. Fig. 5b is the typical output short current of the NCING with a capacitor charge source. It is similar with PVDF electret charge source. Then we changed the capacitor voltage from 5 V to 15 V, testing the output at different voltages. The result is illustrated in Fig. 5c. As shown, the induced current increases synchronously with the voltage of capacitor. For the same capacitor, the larger the voltage, the more charge is stored, and the more charge is induced on the electrode, thus increasing the induced current. Next, the frequency of movement of the charge source (capacitor) and the distance between the charge source and the electrode were changed. We got similar results, as shown in Fig. 5d and e. As the frequency increases or the distance decreases, the short current are both increases. Fig. 5f shows the ability of the NCING to charge a $47 \mu\text{F}$ commercial capacitor and the charging circuit diagram.

3.4. The applications and advantages of NCING

Fig. 6a is a simple device we designed based on NCING that collects water wave energy for sea lighting. The device improves energy conversion efficiency by interdigital electrodes. The fine structure of the device is shown in Fig. S4 in the supporting information. Fig. 6b–c shows the scaling down photographs of the water wave energy collection system. Fig. 6d is the waveform diagram of the output current of the device when collecting water wave energy. The greater the wave, the greater the output current. Thereby, our device can also detect the level of the waves while collecting the wave energy, and give an early warning when the waves are too large. This means that the device has potential application in predicting tidal changes and ocean fluctuations. In such an offshore environment, nanogenerators can be combined with solar cell to provide energy support for specific components, thereby avoiding complex wired energy supply, reducing system cost and offering systematized application.

Non-contact structure produces a lower damping effect, which can be utilized to design a self-powered inertial sensor based on NCING, Fig. 7a is the schematic diagram and the prototype is shown in Fig. 7b. The slider on the slide rail can move freely. The spring is fixed at both ends of the slider to restore the slider to the starting position. The bottom surface of the slider is a charge source, and two electrodes are fixed on the bottom plate directly below the slider. Fig. 7c is the current output waveform of the inertial sensor during an acceleration deceleration process. When the object accelerates, the slider will move backwards relative to the object due to inertia, and the first negative peak will be generated. After the acceleration is over, the slider will return to the initial position under the action of the spring, and a positive peak will be generated. When the object is decelerating, the slider will move forward relative to the object due to inertia, and a positive

peak will be generated. When the object stops, the spring pushes the slider to the initial position, a negative peak will be generated. So it is easy to judge the motion state of the object according to the change of the waveform.

As is known to all, friction generates heat. Therefore, triboelectric nanogenerator will convert part of mechanical energy into heat and reduce energy conversion rate, especially sliding mode triboelectric nanogenerator. We observed the temperature change of PVDF film by infrared camera, as shown in Fig. 8a–b. The temperature of PVDF is the same as the surrounding environment before friction with aluminum foil. After friction, the temperature increased by 20 °C. However, the temperature of PVDF electret has no significant change after NCING working for 2 min, as shown in Fig. 8c–d. This character can be used for forest fire prevention, where additional heat increases risk of adding fire point, as indicated in Fig. S7. Meanwhile, energy can be saved in such configuration. Especially in further development using such configuration, higher converting efficiency may be obtained.

4. Conclusion

A new type of freely slidable NCING was successfully designed. The energy output is produced by the displacement of the charge source in relative to the two electrodes. The charge source and electrode keep from contact. The charge source is not unique and any charged objects such as electrets, charged capacitors, or frictional electrified bodies can be used to generate electricity, providing more possibilities for the field of nanogenerators. The NCING has a simple structure and is easy to manufacture, and provides a possibility for mass production. Moreover, the non-contact configuration generates no additional heat, making it safe in fire prevention applications and reserves possibility for higher energy conversion efficiency. The effectiveness of NCING for powering commercial electronic devices was successfully demonstrated. Water wave energy was successfully collected. Meanwhile, such special configuration can be applied to inertial sensors. In summary, our results demonstrate a new NCING configuration widely developable for low carbon or environmentally friendly self-powered electronics and sensors. Acknowledgements

This work was supported by the National Natural Science Foundation of China (51673103 and 11847135), the Shandong Provincial Natural Science Foundation, China (ZR2017BA013), the China Postdoctoral Science Foundation (2017M612200), and the Postdoctoral Scientific Research Foundation of Qingdao (2016007 and 2016014).

Conflicts of interest

There are no conflicts to declare.

Appendix A. Supplementary data

Supplementary data to this article can be found online at <https://doi.org/10.1016/j.nanoen.2019.103878>.

References

- [1] J. Sun, X. Pu, M. Liu, A. Yu, C. Du, J. Zhai, W. Hu, Z.L. Wang, *ACS Nano* 12 (2018) 6147–6155.
- [2] J. Deng, K. Xiao, R. Liu, W. Ding, A.C. Wang, Y.C. Lai, D. Kai, W. Zhen, Y. Wang, L. Wang, *Adv. Mater.* 30 (2018) 1705918.
- [3] F.R. Fan, L. Lin, G. Zhu, W. Wu, R. Zhang, Z.L. Wang, *Nano Lett.* 12 (2012) 3109.
- [4] F.R. Fan, Z.Q. Tian, Z.L. Wang, *Nano Energy* 1 (2012) 328–334.
- [5] S. Wang, L. Lin, Z.L. Wang, *Nano Lett.* 12 (2012) 6339–6346.
- [6] J. Zhong, Q. Zhong, F. Fan, Y. Zhang, S. Wang, B. Hu, Z.L. Wang, *J. Zhou, Nano Energy* 2 (2013) 491–497.
- [7] G. Zhu, C. Pan, W. Guo, C.Y. Chen, Y. Zhou, R. Yu, Z.L. Wang, *Nano Lett.* 12 (2012) 4960–4965.
- [8] G. Zhang, Q. Liao, M. Ma, F. Gao, Z. Zhang, Z. Kang, Y. Zhang, *Nano Energy* 52 (2018) 501–509.
- [9] C. Chang, V.H. Tran, J. Wang, Y.K. Fuh, L. Lin, *Nano Lett.* 10 (2010) 726.

- [10] X. Chen, S. Xu, N. Yao, Y. Shi, *Nano Lett.* 10 (2010) 2133–2137.
- [11] J. Kwon, W. Seung, B.K. Sharma, S.W. Kim, J.H. Ahn, *Energy Environ. Sci.* 5 (2012) 8970–8975.
- [12] J.H. Lee, K.Y. Lee, B. Kumar, N.T. Tien, N.E. Lee, S.W. Kim, *Energy Environ. Sci.* 6 (2012) 169–175.
- [13] C. Sun, J. Shi, D. Bayerl, X. Wang, *Energy Environ. Sci.* 4 (2011) 4508–4512.
- [14] Z.L. Wang, J. Song, *Science* 312 (2006) 242–246.
- [15] S. Xu, Y. Qin, C. Xu, Y. Wei, R. Yang, Z.L. Wang, *Nat. Nanotechnol.* 5 (2010) 366–373.
- [16] G. Zhu, R. Yang, S. Wang, Z.L. Wang, *Nano Lett.* 10 (2010) 3151.
- [17] Y. Yang, W. Guo, K.C. Pradel, G. Zhu, Y. Zhou, Y. Zhang, Y. Hu, L. Lin, Z.L. Wang, *Nano Lett.* 12 (2012) 2833.
- [18] Y. Yang, J.H. Jung, B.K. Yun, F. Zhang, K.C. Pradel, W. Guo, Z.L. Wang, *Adv. Mater.* 24 (2012) 5357–5362.
- [19] Y. Yang, S. Wang, Y. Zhang, Z.L. Wang, *Nano Lett.* 12 (2012) 6408.
- [20] Y. Yang, Y. Zhou, J.M. Wu, Z.L. Wang, *ACS Nano* 6 (2012) 8456–8461.
- [21] R. Que, M. Shao, S. Wang, D.D.D. Ma, S.T. Lee, *Nano Lett.* 11 (2011) 4870–4873.
- [22] W. Li, D. Torres, T. Wang, C. Wang, N. Sepúlveda, *Nano Energy* 30 (2016) 649–657.
- [23] J. Chen, G. Zhu, W. Yang, Q. Jing, P. Bai, Y. Yang, T.C. Hou, Z.L. Wang, *Adv. Mater.* 25 (2013) 6094–6099.
- [24] K. Dong, J. Deng, Y. Zi, Y.C. Wang, C. Xu, H. Zou, W. Ding, Y. Dai, B. Gu, B. Sun, *Adv. Mater.* 29 (2017) 1702648.
- [25] Y. Hu, C. Xu, Y. Zhang, L. Lin, R.L. Snyder, Z.L. Wang, *Adv. Mater.* 23 (2011) 4068–4071.
- [26] W. Du, J. Nie, Z. Ren, T. Jiang, L. Xu, S. Dong, L. Zheng, X. Chen, H. Li, *Nano Energy* 51 (2018) 260–269.
- [27] J. Nie, Z. Ren, J. Shao, C. Deng, L. Xu, X. Chen, M. Li, Z.L. Wang, *ACS Nano* 12 (2018) 1491–1499.
- [28] L. Tao, J. Zou, X. Fei, Z. Meng, C. Xia, W. Ning, L.W. Zhong, *ACS Nano* 11 (2017) 3950.
- [29] L.-B. Huang, G. Bai, M.-C. Wong, Z. Yang, W. Xu, J. Hao, *Adv. Mater.* 28 (2016) 2744–2751.
- [30] W. Zeng, X.M. Tao, S. Chen, S. Shang, H.L.W. Chan, S.H. Choy, *Energy Environ. Sci.* 6 (2013) 2631–2638.
- [31] Y. Cheng, X. Lu, K.H. Chan, R. Wang, Z. Cao, J. Sun, G.W. Ho, *Nano Energy* 41 (2017) 511–518.
- [32] M.R. McDevitt, D.S. Ma, L.T. Lai, J. Simon, P. Borchardt, R.K. Frank, K. Wu, V. Pellegrini, M.J. Curcio, M. Miederer, N.H. Bander, D.A. Scheinberg, *Science* 294 (2001) 1537–1540.
- [33] X. Wang, W.-Z. Song, M.-H. You, J. Zhang, M. Yu, Z. Fan, S. Ramakrishna, Y.-Z. Long, *ACS Nano* 12 (2018) 8588–8596.
- [34] Y. Zi, L. Lin, J. Wang, S. Wang, J. Chen, X. Fan, P.K. Yang, F. Yi, Z.L. Wang, *Adv. Mater.* 27 (2015) 2340–2347.
- [35] L. Lin, Y. Xie, S. Niu, S. Wang, P.-K. Yang, Z.L. Wang, *ACS Nano* 9 (2015) 922–930.
- [36] G. Zhu, J. Chen, T. Zhang, Q. Jing, Z.L. Wang, *Nat. Commun.* 5 (2014) 3426.
- [37] Y. Xie, S. Wang, S. Niu, L. Lin, Q. Jing, J. Yang, Z. Wu, Z.L. Wang, *Adv. Mater.* 26 (2014) 6599–6607.
- [38] S. Wang, Y. Xie, S. Niu, L. Lin, Z.L. Wang, *Adv. Mater.* 26 (2014) 2818–2824.
- [39] H.-J. Qiu, W.-Z. Song, X.-X. Wang, J. Zhang, Z. Fan, M. Yu, S. Ramakrishna, Y.-Z. Long, *Nano Energy* 58 (2019) 536–542.
- [40] W. Paosangthong, R. Torah, S. Beeby, *Nano Energy* 55 (2019) 401–423.
- [41] V. Nguyen, R. Zhu, R. Yang, *Nano Energy* 14 (2015) 49–61.



Wei-Zhi Song received his BS degree from Qingdao University in 2017. Now he is studying for his master's degree at Qingdao University (with Prof. Yun-Ze Long). His current research interests are focused on electrospinning techniques, nanogenerator and their applications.



Xiao-Xiong Wang received the Ph.D. degree in University of Science and Technology of China in 2016. His research fields cover electrospinning of magnetic materials, electrospun nanogenerators and their applications, infrared radiative cooling materials.



Hui-Jing Qiu received her BS degree from University of Jinan in 2017. Now he is studying for her master's degree at Qingdao University (with Prof. Yun-Ze Long). Her current research interests are focused on triboelectric nanogenerator and self-powered electronics.



Miao Yu graduated from Nanjing University (Bachelor of Physics) with a master's degree. He got the master's degree from Hong Kong University of Science and Technology (Master of Electronic Materials). He has a doctoral degree from Columbia University (PhD in Physics and Materials Engineering). In 2016, he was selected as a leader in Taishan industry in Shandong Province (Taishan scholars from overseas experts in Shandong Province). His research interests focus on electrospinning and nanomaterials.



Liuqi received his B.S. degree in Qingdao University in 2017. He started M.S. studies in Qingdao University from the fall of 2017. His research interests are mainly about electrospinning and device applications of nanofiber.



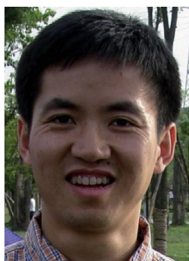
Seeram Ramakrishna is the Vice President of the National University of Singapore (Research Strategy); Dean of the School of Engineering; Founding Director of NUSNNI, Bioengineering; Founding Chairman of the Global Engineering Dean's Council; Vice President of the International Federation of Engineering Education Societies; Member of the Council of the Asian Society for Innovation and Policy. His research areas cover nanomaterials for healthcare, energy, water and environment.



Jun Zhang received the Ph.D. degree in Nankai University in 2016. His research interests cover synthesis of luminescent materials, regulating optical properties of these luminescent materials in electrospun nanofibers and electrospun nanofibers, such as fluorescent materials embedded in nanofibers for optical data storage applications, and Ag nanoparticles embedded in nanofibers for sensing application.



Han Hu, a doctoral tutor at China University of Petroleum. In 2014, he received his Ph.D. from Dalian University of Technology. 2017–2018, Young Researcher, University of Queensland, Australia. The main research directions are new carbon materials, new energy materials, electrochemical energy storage materials and devices.



Zhi-Yong Fan received his BSc and MSc degree from Fudan University, China, in 1998 and 2001, respectively. He received a PhD degree from the University of California, Irvine in 2006. From 2007 to 2010, he worked in the University of California, Berkeley as a postdoctoral fellow, with a joint appointment with the Lawrence Berkeley National Laboratory. In May 2010, he joined the HKUST as an Assistant Professor. His research effort concentrates on engineering novel nanostructures with functional materials, for technological applications including energy conversion, electronics and sensors.



Yun-Ze Long received his BSc degree from the University of Science & Technology of China in 2000 and received a PhD degree from the Institute of Physics, Chinese Academy of Sciences in 2005. He then worked in the Institut des Matériaux Jean Rouxel, CNRS, France, as a postdoctoral fellow. He has been with the Qingdao University since Dec. 2006, where he is currently a full Professor. From 2009 to 2011, he worked as a visiting researcher in the University of Sydney and the HKUST. His research interests focus on one dimensional functional nanomaterials.